High Areal Capacity Battery Electrodes Enabled by Segregated Nanotube Networks

Sang-Hoon Park,[1,2] Paul J. King,[1,3] Ruiyuan Tian,[1,4] Conor S. Boland,[1,4] Joao Coelho,[1,2] Chuanfang (John) Zhang,[1,2] Patrick McBean,[4] Niall McEvoy,[1,2] Matthias P. Kremer,[1,2] Dermot Daly,[1,2] Jonathan N. Coleman[1,4,*] and Valeria Nicolosi[1,2,*]

[1]*CRANN and AMBER research centers, Trinity College Dublin, Dublin 2, Ireland*

[2]*School of Chemistry, Trinity College Dublin, Dublin 2, Ireland*

[3]*Efficient Energy Transfer Department, Bell Labs Research, Nokia, Blanchardstown Business & Technology Park, Snugborough Road, Dublin 15, Ireland*

[4]*School of Physics, Trinity College Dublin, Dublin 2, Ireland.*

**colemaj@tcd.ie (Jonathan N. Coleman), Tel: +353 (0) 1 8963859,*

**nicolov@tcd.ie (Valeria Nicolosi), Tel: +353 (0) 1 8964408.*

Abstract

Increasing the energy storage capability of lithium-ion batteries necessitates maximization of their areal capacity. This requires thick electrodes performing at near-theoretical specific capacity. However, achievable electrode thicknesses are restricted by mechanical instabilities, with high-thickness performance limited by the attainable electrode conductivity. Here we show that forming a segregated network composite of carbon nanotubes with a range of lithium storage materials (e.g. silicon, graphite and metal oxide particles) suppresses mechanical instabilities by toughening the composite, allowing the fabrication of high-performance electrodes with thicknesses of up to 800 μm. Such composite electrodes display conductivities up to 10^4 S m^{-1} and low charge-transfer resistances, allowing fast charge-delivery and enabling near-theoretical specific capacities, even for thick electrodes. The combination of high thickness and specific capacity leads to areal capacities of up to 45 and 30 mAh cm^{-2} for anodes and cathodes respectively. Combining optimized composite anodes and cathodes yields full-cells with state-of-the-art areal capacities (29 mAh cm^{-2}) and specific/volumetric energies (480 Wh kg^{-1} and 1600 Wh L^{-1}).

Introduction

To meet trends such as the rise of electric vehicles, significant advances in the energy storage capability of batteries are urgently required. In the dominant field of lithium-ion batteries, most research has focused on the development of high-capacity electrode materials such as silicon for the anode or lithium sulfide for the cathode.[1] An alternative strategy would be to optimize electrode architecture to maximize the electrode areal capacity (C/A), thus increasing energy density. For both anodes and cathodes, $C/A = C_{SP} \times M/A$, where C_{SP} is the specific capacity (mAh g^{-1}) of the electrodes and M/A is its mass loading (g cm^{-2}). Thus, both C_{SP} and M/A must be simultaneously maximized, leading to a number of challenges. First, high-performance electrode materials tend to be granular (i.e. particulate-based) and so display mechanical instabilities above the so-called critical cracking thickness (CCT),[2,3] making it impossible to prepare very thick electrodes even with polymeric binders. Secondly, poor conductivity of advanced electrode materials means conductive additives must be incorporated to allow charge distribution within the electrode. Standard additives such as carbon black (CB) yield low, inhomogeneous and unstable electrode conductivity,[3-5] limiting electrochemical performance, especially for very thick electrodes.[6]

While a number of methods have been suggested to maximize C/A,[7-16] none are scalable. We aim to develop a general, materials science-based strategy that allows the production of very thick electrodes which retain almost all of their theoretical capabilities. Such a strategy must involve simple and scalable production techniques, should apply to both anodes and cathodes and be compatible with any high-performance electrode material.

Here, we show that the goals outlined above can be achieved *via* simultaneously boosting the electrical/mechanical properties of granular electrode materials by using carbon nanotubes (CNT), specifically in the form of segregated networks, as both binder and conductive additive, without any additional polymer or CB. By adding nanotubes to high-performance, yet low cost commercial anode/cathode materials such as micron-sized-silicon (μ-Si) and $LiNi_xMn_yCo_zO_2$ (NMC), we demonstrate a hierarchical composite where the nanotubes arrange themselves into networked membranes that envelop the active material particles. These networks dramatically improve the mechanical properties, allowing the fabrication of very thick electrodes, as well as improving their stability, even during repeated charge/discharge. At the same time, the electrode conductivity is radically increased, facilitating fast charge distribution, even in thick electrodes. This allows us to produce extremely thick (up to 800 μm) electrodes with C_{SP}

approaching theoretical values for each electrode material. This enables the production of full-cells with areal capacities and specific energies considerably higher than any previous reports.

Segregated network composites

Here we show that micron-sized particles of standard lithium-storing materials can be formed into robust electrodes by mixing with small amounts of carbon nanotubes without any additional polymeric binder or conductive additive. Initially, we focus on micron-sized silicon (μ-Si) particles which combine high specific capacity (3579 mAh g^{-1}) with low cost (Supplementary Fig. 1). We found that extremely robust μ-Si/CNT composite electrodes can be produced directly on Cu substrates by a simple, scalable slurry-casting technique (Fig. 1a and see XRD and Raman analysis in Supplementary Figs. 2−3). Critically, all our slurries are water-based and utilise no organic solvents, significantly simplifying waste management.

Interestingly, these composites do not display the usual network structure found in CNT-based nanocomposite electrodes,[17,18] but rather display the much less well-known segregated network structure.[19] Such networks occur for particulate matrices with particle sizes which are larger than the filler (nanotube) length (here ~1 μm). Then the excluded-volume associated with the particles drives the formation of a segregated network,[19] where the CNTs form networked 2-dimensional membranes which wrap and interconnect the active material (AM) particles (Fig. 1b), even at extremely low CNT mass-fractions (M_f).[19] Cross-sectional SEM images of μ-Si/CNT (here 5 μm Si particles) anodes at the different CNT M_f show the progressive development of 2D CNT-membranes, with hierarchical structure appearing at ~1wt% and membranes becoming progressively denser/thicker as more CNTs are added (Figs. 1c−e and more SEM images in Supplementary Figs. 4−5). Critically, such hierarchical structures do not form for composites containing small particles (i.e. 80 nm nano-Si, Fig.1f and Supplementary Fig. 6) and clearly require large particle-size/nanotube-length ratios. High-magnification imaging shows the membranes to effectively wrap the Si particles and consist of entangled, van der Waals bonded networks of CNT bundles/ropes[20] (Figs. 1g−h and Supplementary Fig. 7). Such structures are expected to be particularly useful in battery electrodes due to their ability to simultaneously enhance conductivity and mechanical toughness,[21] facilitate particle expansion as well as localizing Si fragments in the event of pulverization while allowing easy access of lithium ions.

Versatility of segregated network battery electrodes

We found that segregated network composites (SNCs) can be produced by mixing CNTs with a wide range of micron-particle-size battery materials (e.g. μ-Si, NMC, graphite and LTO). To illustrate this, Fig. 2 shows data for SNCs using two types of NMC, μ-Si of three different sizes as well as a non-segregated network composite based on nano-Si for comparison (see Fig. 2a for images of active materials and Supplementary Figs. 8−14 for SNC images).

With regards basic characterisation, the in-plane electrical conductivity of SNCs displayed very large increases at relatively low M_f's (Fig. 2b), with higher conductivities observed for larger particle sizes as expected[19] and the non-segregated network showing the lowest in-plane conductivity. Critically, SNC in-plane conductivities were orders of magnitude larger than traditional electrodes at near equivalent compositions.

To examine the SNC conductivity in more detail, we performed electrochemical impedance spectroscopy on 2μm-Si anodes with various nanotube M_fs. Fitting the spectra to a standard model,[22,23] consisting of the electrolyte resistance, a Warburg impedance and two resistance/constant phase element combinations, representing the electrode and charge-transfer resistances (see Supplementary Fig. 15 and Table 1), yielded the electrolyte, electrode and charge transfer resistances which are plotted *versus* M_f in Fig. 2c. We find increasing the CNT content yields dramatically decreased electrode and charge-transfer resistances. For M_f>0.25wt%, both $R_{Electrode}$ and R_{CT} were superior to traditional electrodes of 2μm-Si with 20% CB/PAA.

We converted the electrode resistance to a conductivity via the electrode dimensions. For comparison, we measured the out-of-plane electrode conductivity, $\sigma_{Out-of-plane}$, reasoning that this parameter to be most relevant to charge transport during battery operation. Although $\sigma_{Out-of-plane}$ was approximately ×1000 lower than $\sigma_{In-plane}$, it was very close to $\sigma_{Electrode}$ (Fig. 2d) with both parameters scaling with percolation theory,[18] ($\sigma \propto (M_f - M_{f,c})^n$) where $M_{f,c}$=0.18wt% and n=0.65. Taken together, this data confirms that adding CNT significantly improves the electrochemical performance of electrodes and identifies the out-of-plane conductivity as an important material parameter.

We found SNCs to perform very well as lithium-ion battery anodes (Fig. 2e−g). For all Si particle sizes, the 1st-cycle delithiation capacity (normalized to Si mass, C/M_{Si}) showed near-

theoretical values and very high Columbic efficiencies (85−90%, see Supplementary Fig. 16) once M_f>2wt% (Fig. 2f). For both types of NMC, near-theoretical capacities were observed at M_f as low as 0.25%. We attribute these high capacities to the extremely high conductivities associated with SNCs. The data in Fig 2b and e implies the theoretical capacity to be reached for both Si- and NMC-based electrodes once $\sigma_{In-plane}$ surpasses ~100 S/m ($\sigma_{Out-of-plane}$ > ~0.1 S/m).

Shown in Fig. 2g is 1st-cycle specific capacity data for μ-Si-based SNC electrodes with an optimised nanotube content (M_f=7.5wt%, see Supplementary Fig. 17), plotted *versus* μ-Si particle size. We find near theoretical capacities for all sizes up to 45 μm. Such high capacities have never before been observed for such large particles. This data contrasts with traditional Si/polymer/CB anodes (80:10:10) which showed a large fall-off in the 1st-cycle capacity as the Si particle size was increased. In addition, SNC-based electrodes showed very high capacities, even after 20 cycles for particle sizes up to 2 μm, although larger particle sizes show significantly poorer stability (Fig. 2g). Because material cost decreases significantly with particle size (see Supplementary Fig. 18 and Table 2), we will focus on 2μm Si for the rest of the study.

Although the optimised SWNT content for 2μ-Si-based SNC electrodes (7.5wt%) was much lower than the additive contents in traditional electrodes, it is not inconsequential and could have a non-trivial impact on the electrode cost. However, it is worth noting that for 2μ-Si electrodes, high capacities were also achieved for M_f=2wt% (Fig. 2f and S16) while for NMC based cathodes, optimised loadings were smaller (0.5wt%), due to the larger particle size. This suggests it will be possible to develop SNC-based electrodes that are economically viable.

Segregated networks lead to extremely thick electrodes

When trying to obtain high C/A, an almost universally underestimated problem is how to achieve very thick electrodes (i.e. high M/A). When granular materials are deposited as films from liquids, large capillary pressures leading to significant drying stresses.[2,3] Such stresses lead to catastrophic cracking above the critical cracking thickness, the magnitude of which depends on the mechanical properties of the film.[2] Traditional polymer binder/CB combination yields relatively poor reinforcement (see Supplementary Fig. 19), leading to mediocre mechanical properties and so low CCTs of <175 μm (see Supplementary Fig. 20−21). This problem is largely unappreciated and significantly limits achievable thickness. In addition, in

traditional polymer/CB-loaded electrodes, we found conductivity and toughness to be anti-correlated (see Supplementary Fig. 19) making it impossible to prepare conductive yet tough electrodes.

However, tensile tests show the mechanical properties of SNC-based electrodes to be far superior to traditional electrode materials (Fig. 3a-b and Supplementary Fig. 19). Of particular interest is the tensile toughness (work done at failure per volume, see Fig. 3c) which has been linked to electrode stability in a study which showed tough electrodes to be crack-resistant.[18] We observed very large increases of toughness with CNT M_f, leading to SNCs which were >500 times tougher than the traditional electrodes for similar compositions. Interestingly, the 80nm-Si-based non-segregated networks showed considerably lower toughness increases, highlighting the importance of SNCs. All electrodes showed toughness increases which were consistent with percolation theory (i.e. $T \propto (M_f - M_{f,c})^n$, solid lines)[21] with percolation thresholds, $M_{f,c}$, which decrease with increasing particle size as expected for segregated networks[19] ($M_{f,c}$=0.17wt% for 2μm Si/CNT, similar to the conductivity data). Such mechanical percolation has been observed previously in non-segregated nanotube networks where large-scale nanotube network formation has occurred.[21] Importantly, unlike the traditional electrodes, toughness and conductivity are correlated in SNCs allowing the production of electrodes which are much tougher and more conductive compared to traditional systems (Fig. 3d, see also SNCs with different CNTs in Supplementary Fig. 22).

As shown in Fig. 3e, traditional polymer-stabilised electrodes display CCTs of <175 μm, limiting achievable thickness and so areal capacity (typically, <4 mAh cm^{-2}, see below). We find severe cracking to occur for traditional electrodes with thickness >CCT. However, the high toughness associated with the SNCs yields much higher CCTs, allowing the production of mechanically robust electrodes (Fig. 3f-h) with thicknesses as high as ~300 μm for μ-Si/CNT and ~800 μm for NMC/CNT SNCs (see Supplementary Fig. 23 for thick electrodes based on other active materials). These thicknesses are much larger than achievable with traditional binders. In addition, we note that Fig 3f-g shows the density of the μ-Si/CNT electrode to be 0.7 g cc^{-1}, consistent with a SNC porosity of ~70%, enough to accommodate the expansion of silicon during charging with minimal dimensional change of the overall electrode.

High areal capacity of segregated network electrodes

We believe the combination of high toughness and conductivity shown in Fig. 3c is critical for high capacity electrodes: the mechanical reinforcement facilitates the formation of very thick electrodes while the conductivity enhancement enables rapid charge-delivery, yielding capacities close to the theoretical limit. Critically, because $C / A = C_{SP} \times M / A$, achieving high areal capacity requires achieving near-theoretical capacity and high electrode thickness simultaneously.

To demonstrate that high C/A can be achieved using SNCs, we produced sets of 2 μm Si/7.5wt%CNT anodes and NMC811/0.5%CNT cathodes, each with varying the M/A up to 15 mg cm^{-2} and 155 mg cm^{-2}, respectively (i.e. thicknesses of 210 μm and 740 μm. (N.B. thicker anodes with 22 mg cm^{-2} were made but couldn't be tested in half-cells due insufficient Li in the cathode). Galvanostatic charge-discharge (GCD) measurements (Fig. 4a−b) yielded specific capacities which were invariant with mass loading for both anodes and cathodes with values close to the respective theoretical values (Fig. 4c−d).

The combination of near-theoretical capacities and high electrode thicknesses leads to extremely high areal capacities which scale linearly with mass loading over the entire thickness range (Fig. 4e-f), with the slopes yielding total specific capacities of 3150 and 185 mAh g^{-1}. For the thickest electrodes, C/A reached values of 45 and 29 mAh cm^{-2}, well beyond the state-of-the-art (open stars represent literature values, see Supplementary Table 3−5).[9-11,24-29]

The disconnection of silicon from the electrode due to crack-formation is a known capacity-loss mechanism in Si-based LiBs.[30] These extremely thick electrodes are relatively stable (Fig. 4g-h), partly because the CNT membrane prevents electrode cracking during repeated cycling.[18] Post-mortem analysis after cycling (see Supplementary Fig. 24) shows that the CNT-membrane has been preserved with a little change in the hierarchical structure, while Li-metal counter electrode shows severe degradation (see Li-metal degradation issue in Supplementary Fig. 25). Although XRD and SEM (see Supplementary Fig. 24) show pulverisation to occur in μ-Si/SNC-based electrodes, the resultant silicon particles are contained within the nanotube membranes associated with the SNC and so remain available to store charge.

Unsurprisingly for such thick electrodes and relatively large AM particles,[6] we do observe some capacity falloff at high charge/discharge rates (Fig. 4i-j). However, reasonable combinations of capacity and current can be achieved, presumably because the high conductivity associated with the segregated nanotube network allows fast charge distribution.

Full-cell performance

The ability to produce both anodes and cathodes with very high areal capacities allows us to produce high-performance full-cells. By keeping the anode/cathode thickness ratios at the level required to match areal capacities but increasing the total anode plus cathode mass loading, $(M/A)_{A+C}$, we produced full-cells with record cell areal capacity, $(C/A)_{Cell}$, up to 29 mAh cm^{-2} (Fig. 5a and see full-cell information in Supplementary Fig. 26 and Table 6). It is worth noting that the full-cell $(C/A)_{Cell}$ is limited by the cathode (Maximum cathode C/A was 30 mAh cm^{-2} while for anodes we achieved C/A up to 45 mAh cm^{-2}), reinforcing the need to develop high-C_{SP} cathode materials.

These full-cells were relatively stable, showing >80% retention after 50 cycles at 1/15 C-rate and >95% retention after 150 cycles at 1/3 C-rate (see Fig. 5b and long-term cycling in Supplementary Fig. 27). While these results are competitive with most μ-Si-based studies, we note that typical issues associated with the electrode/electrolyte interface (i.e. unstable SEI, electrolyte depletion, etc.) were not addressed in this work as we have focused on electrode architecture. This means there is further scope to improve stability, e.g. by optimizing electrolyte composition.[31]

The charging/discharging rate-capabilities of our high-C/A full-cells are shown in Fig. 5c-d, and yield similar results to the individual electrodes. Inevitably, we find reduced rate performance for the thickest electrodes.[6] However, even though our high-rate capacity was approximately ×3 below the low-rate C/A (~30 mAh cm^{-2}) for the thickest electrodes, such cells still deliver ~10 mAh cm^{-2} within ~1 hour, during both charging and discharging. This is greater than almost all traditional electrodes (<3 mAh cm^{-2}) at the similar rate,[32-34] and fast enough for realistic applications.[35] By converting the data in Fig. 5d into a Ragone plot (Fig. 5e), it is clear that the combination of energy and power associated with SNC-based full cells is superior to traditional electrodes.

Another advantage of these composites is that, because the electrodes can be made so thick, the inactive components (Al/Cu foils, separator, electrolyte filled in the electrodes, etc.) become a very small fraction of the whole (see Supplementary Table 6), thus increasing the overall energy density. Considering the mass of both electrodes and all the inactive components (i.e. current collectors, electrolyte and separator), we have calculated the specific energy, E_{SP}, for our full-cells, along with high-C/A cells from other studies and plotted it *versus* the

corresponding full-cell $(C/A)_{cell}$ in Fig. 5f (see calculations and literatures in Supplementary Table 6−7).[9,32-34,36] This plot shows that our high-C/A full-cells delivered much higher E_{SP} (up to 401 Wh kg^{-1}) than any other reports (<261 Wh kg^{-1}, open symbols), highlighting their superlative performance. We note that, after calendaring to increase the density of both electrodes by ~60% and so decrease electrolyte mass, we could increase the energy density up to 480 Wh kg^{-1}, a value which is nearly twice the state-of-the-art (see Supplementary Table 7).

The relationship between E_{SP} and $(C/A)_{Cell}$ can be illustrated *via* a simple relationship (see derivation in Supplementary Note 1):

$$E_{SP} = \frac{V}{\frac{1}{C_{SP,Cathode}} + \frac{1}{C_{SP,Anode}} + \frac{(M/A)_{Inactive}}{(C/A)_{Cell}}} \quad (1)$$

where V, $C_{SP,Cathode}$, $C_{SP,Anode}$ and $(M/A)_{Inactive}$ are the average operating voltage, cathode/anode gravimetric capacity and the inactive components' M/A. Plotting equation 1 for each system shows the curves saturate at high $(C/A)_{Cell}$ at a value determined by C_{SP} of the lower performing electrode, generally the cathode. As shown in Fig. 5f, the curve representing our data approaches 401 Wh kg^{-1} at the highest $(C/A)_{Cell}$ achieved (29 mAh cm^{-2}), close to saturation. This means that the composite architecture has allowed us to approach the absolute maximum C_{SP} possible for the cathode material used. This implies that once more advanced cathode materials (e.g. Li_2S) become widely available, this approach would be expected to allow commensurate increases in E_{SP}.

Finally, we have estimated the volumetric energy density of our highest M/A_{C+A} full cells to be 1030 Wh L^{-1}, increasing to 1600 Wh L^{-1} on calendaring (see Supplementary Fig. 28). This value is >60% higher than the state-of-the-art (<972 Wh L^{-1}),[37] demonstrating the superlative cell-level performance enabled by SNCs.

Conclusions

While nanotubes have been used before to improve electrode conductivity,[17,18] segregated networks - which are much more appropriate to realistic electrode materials - have not been utilised in battery electrodes (see Supplementary Table S8). In addition to considerable conductivity enhancement, these networks dramatically increase mechanical robustness, allowing the production of extremely thick electrodes with very high areal capacities.

Combining segregated network-based anodes and cathodes leads to full-cells with specific and volumetric energy densities of 480 Wh kg^{-1} and 1600 Wh L^{-1}, respectively. We consider segregated network composite-based electrodes as a general solution for the production of high capacity battery electrodes.

Methods

Composite Electrode Fabrication

The hierarchical composite electrodes were prepared *via* a conventional slurry-casting method using a CNT aqueous dispersion (0.2 wt% SWCNT in water, ~0.2 wt% PVP as a surfactant stabilizer, Tuball, OCSiAl) and battery active materials (AMs) without any additional polymeric binder or carbon black (CB).

For anodes, the CNT dispersion was mixed with micron-sized Si powder (μ-Si) with a range of particle sizes (1−3 μm: denoted as 2 μm and 5, 10, 30, 45 μm size, all purchased from US Research Nanomaterials) and ground into a uniform slurry using a mortar and pestle. The CNT mass fraction, (M_f) in the resultant electrodes was controlled in the range of 0.05−20 wt% by simply changing the mass ratio between the μ-Si and CNT dispersion. For instance, 8 ml of CNT dispersion was mixed with 200 mg of μ-Si in order to obtain the electrode with 7.5 wt% CNT. Then the slurry was cast onto copper (Cu) foil using a doctor blade, then slowly dried at 40 °C for 2 hours and followed by vacuum drying at 100 °C for 12 hours to remove residual water. To remove the PVP surfactant from the as-received CNT dispersion (~0.2 wt% PVP), the dried electrodes were then heat-treated in Ar gas at 700 °C for 2 hours. By changing the height of doctor blade (200−2000 μm) while keep the CNT M_f constant, we obtained electrodes with various thickness, ranging from 30−310 μm (M/A = 0.9 – 21.5 mg cm^{-2}).

For cathodes, we employed NMC (NMC532: $LiNi_{0.5}Mn_{0.3}Co_{0.2}O_2$ or NMC811: $LiNi_{0.8}Mn_{0.1}Co_{0.1}O_2$, MTI Corp.) to mix with the CNT aqueous dispersion. Typically, 5 ml of CNT was ground with 2 g of NMC to obtain the electrode with 0.5 wt% CNT. The resultant slurry was cast onto aluminium (Al) foil and dried at the same manner. We also controlled CNT M_f in the range between 0.01 − 10 wt% and varied electrode thickness, ranging from 40 − 800 μm (M/A = 6 − 155 mg cm^{-2}). The composite anode/cathode were denoted as "μ-Si/CNT" and "NMC/CNT", respectively.

For comparison, we employed nano-sized Si (n-Si) with different sizes (~25 nm and ~80 nm, US Research Nanomaterials), to fabricate corresponding anodes by mixing with CNT dispersion in desired compositions and thicknesses.

In addition, traditional electrodes were also prepared using carbon black (Timical Super C65, MTI Corp.) and conventional binders, either PAA (Sigma Aldrich) for Si anode or PVDF (EQ-Lib-PVDF, MTI Corp) for NMC cathode. Electrode thickness and composition were also controlled in the same manner.

Material Characterization

The morphology and micro-structure of Si/CNT anodes (or NMC/CNT cathodes) were examined by FE-SEM (Zeiss Ultra Plus, Zeiss) in a high vacuum mode with an acceleration voltage of 5 keV. The mass (M) and thickness (t) of the electrodes were determined using a microbalance (MSA6, Sartorious) and a digital micro-meter after subtracting the mass or thickness of the Al/Cu foils.

The structural properties of samples were characterized by X-ray diffraction (XRD, Bruker D5000 powder diffractometer) with a monochromatic Mo Kα radiation source (λ = 0.15406 nm). XRD patterns were collected between $10° < \theta < 80°$, with a step size of 2θ = 0.05° and a count time of 12 s/step.

Raman spectra of composite electrodes were acquired using a Witec Alpha 300 R with a 532 nm excitation laser and a spectral grating with 600 lines mm^{-1}. Characteristic spectra were obtained by averaging 20 discrete point spectra for each sample. Raman maps were generated for AM/CNT composites by acquiring 120 × 120 discrete spectra over an area of 60 × 60 μm. Maps representing the presence of CNT and AM (either Si or NMC) were generated by mapping the intensity of the CNT G band and the AM's characteristic band (Si at 520 cm^{-1} or NMC A_{1g} band).

The in-plane electrical conductivity of electrodes was measured using a four-point probe technique while the out-of-plane conductivity was measured using 2-probe. The samples were prepared by the same slurry-casting method but they were coated onto a glass plate instead of Al/Cu foils to exclude the substrates' conductivity. Then, four parallel contact lines were deposited on the electrode surface using silver paint (Agar Scientific). The resistance of samples was measured using a Keithley 2400 source meter. The conductivity of samples was then calculated using the samples' geometric information (electrode area and thickness) obtained by digital calliper/micro-meter.

The mechanical measurements were conducted from free-standing samples using a Zwick Z0.5 Pro-Line Tensile Tester (100 N Load Cell) at a strain rate of 0.5 mm min^{-1}. The films were prepared by simply peeling off the electrodes from the substrate. Each data point was obtained by averaging the results from four independent measurements.

Electrochemical Characterization

The electrochemical properties of the electrodes were investigated using 2032-type coin cells (MTI Corp.) assembled in an Ar-filled glovebox (UNIlab Pro, Mbraun). Each working electrode was punched into discs with diameter = 12 mm. A Celgard 2320 was used as the separator for all coin cells.

For the half-cell electrochemical characterisation, the coin cells were assembled by pairing the working electrode with a Li-metal disc (diameter: 14 mm, MTI Corp.), the latter was used as the counter/reference electrode. 1.2 M lithium hexafluorophosphate ($LiPF_6$) in ethylene carbonate/diethyl carbonate/fluoroethylene carbonate (EC/DEC/FEC, 3:6:1 in v/v/v, BASF) with 2 wt% vinylene carbonate (VC, Sigma Aldrich) was used as the electrolyte for half-cell measurement.

Impedance measurements were performed using a a BioLogoc VMP-30O with a frequency range of 1 MHz – 0.1 Hz and a voltage amplitude of 10 mV. EC-Lab Z-Fit software was used to model the acquired spectra. The electrochemical properties of the Si anodes were measured within a voltage range of $0.005 - 1.2$ V using Galvanostatic charge/discharge mode by a potentiostat (VMP3, Biologic). The NMC cathodes were measured within a voltage range of $3 - 4.3$ V in the same manner. We note that the terms charging/discharging apply to the full-cell LiB system. For the anode, charging/discharging correspond to the lithiation/delithiation process, respectively. The areal capacities (C/A) of the electrodes were obtained by dividing the measured cell capacity by the geometric electrode area (1.13 cm^2). To investigate the maximum accessible C/A of the electrodes, the cells were tested at a reasonably slow condition of 1/30 C-rate. The cyclabilities of the electrodes were evaluated at 1/15 C-rate after initial formation cycle at 1/30 C-rate. The discharge rate-capabilities of the electrodes were investigated using asymmetric charge/discharge conditions; the cells were charged at a fixed 1/30 C-rate then discharged at varied rates. For the post-mortem analysis, the cycled cells were carefully disassembled inside a glove box under inert atmosphere. The cycled electrodes were then rinsed with dimethyl carbonate (DMC) several times and dried inside the glove box at room temperature.

The full-cells were assembled by pairing our μ-Si/CNT anodes with NMC/CNT cathodes with various C/A (or M/A). We used the same sized cathode/anode disc (1.13 cm^2) to match the C/A of both electrodes, which were previously determined in the half-cell experiments. For full-cells, 1.2 M $LiPF_6$ in ethylene methyl carbonate/fluoroethylene carbonate (EMC/FEC, 95:5 in wt%, BASF) was used as the electrolyte.[38] The N/P ratio, defined by the capacity ratio

between the anode and cathode, was balanced to be ~1.1 [See Supplementary Table S6. for the details of cathodes/anodes in full-cells]. The assembled full-cells were then cycled at 1/15 C within a voltage range of 2.5 − 4.3 V after the initial formation cycle at 1/30 C-rate. The total C/A of the full-cell, (full-cell C/A), was obtained by dividing the measured cell capacity by the geometric electrode area (1.13 cm^2). The charging and discharging rate-capabilities of full cells were measured separately using asymmetric charge/discharge protocols. The discharge rate capabilities were investigated by constant current (CC) discharging; the cells were fully charged at ~1/30 C-rate (to reach ~100% of state of charge), then discharged at varied current densities (CC mode). The charge rate capabilities were measured by constant current-constant voltage (CC-CV) charging; the cells were fully discharged at 1/10−1/20 C-rate to reach ~0% of stage of charge, then charged at the different rates with CC-CV mode. The CV mode held until the current had decayed to the 1/10−1/20 C current of each cells. For the sake of comparison, a traditional full-cell (C/A~3.5 mAh cm^2) was also assembled and tested in the same manner by pairing the NMC cathode (C/A = 3.5 mAh cm^{-2}) and graphite anode (C/A = 3.8 mAh cm^{-2}) prepared by CB-binder combination.

Data Availability: The datasets generated during and/or analysed during the current study are available from the corresponding author on reasonable request.

Acknowledgments

All authors acknowledge the SFI-funded AMBER research center (SFI/12/RC/2278) and the Advanced Microscopy Laboratory for the provision of their facilities and acknowledge Romina Charifou, who performed XRD for the samples. JNC thanks Science Foundation Ireland (SFI, 11/PI/1087), the European Research Council (AdvGr FUTUREPRINT) and the Graphene Flagship (grant agreement n°785219) for funding. VN thanks the European Research Council (SoG 3D2D Print) and Science Foundation Ireland (PIYRA) for funding.

Author contributions

S.-H.P., P.J.K., J.N.C, and V.N. conceived the project. S.-H.P. and P.J.K. designed materials and experiments. S.-H.P. and P.J.K. fabricated composite electrodes. S.-H.P. performed electrochemical characterization. N.M performed Raman analysis. S.-H.P., P.J.K. J.C. and R.T.

analyzed electrochemical data. J.C. and D.D. performed electron microscopic analysis. S.-H.P. and J.C.-F.Z measured electrical conductivity. C.B and P.M performed mechanical measurement. S.-H.P. and J.N.C. wrote manuscript. All authors discussed the results and commented on the manuscript.

Financial and non-financial competing interest

Authors declare no competing interests.

Figures

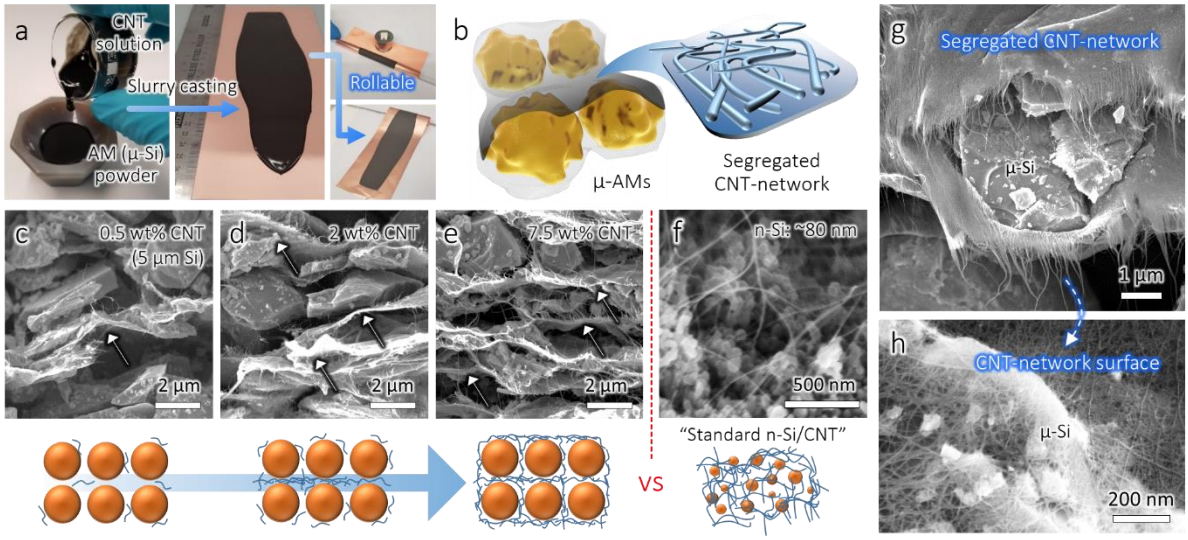

Figure 1. Fabrication of hierarchical composite electrodes. (a) Composite electrode fabrication by mixing aqueous CNT dispersions with particulate active material powders and slurry-casting onto substrates to yield robust, flexible electrodes. **(b)** Schematic of resultant hierarchical Si/CNT segregated network composite electrode, showing formation of 2D CNT-membranes between micron-sized Si (μ-Si) particles. **(c-f)** Cross-sectional SEM images of **(c-e)** μ-Si (5 μm)/CNT segregated network composite anodes with mass fraction (M_f) varying from 0.5–7.5wt% with **(f)** a non-segregated network composite of nano-Si (80 nm)/CNT (M_f=7.5wt%) for comparison. For the segregated network composites, the development of nanotube membranes (arrows) can be clearly seen as M_f increases **(c-e)**. The schemes below illustrate the evolution of the CNT-membranes as the M_f is increased and highlight the difference between normal and segregated network composites. Si particles and CNTs are represented by spheres and bendy rods respectively. **(g-h)** High magnification cross-sectional SEM images of μ-Si/7.5wt% CNT composite anode showing **(g)** a μ-Si particle wrapped by 2D CNT-membranes which consist of entangled, van der Waals bonded networks of CNT bundles/ropes **(h).** Clearly, the membranes are quasi-continuous and so can localize the silicon particles yet contain small (~10 nm) pores which allow free movement of electrolyte.

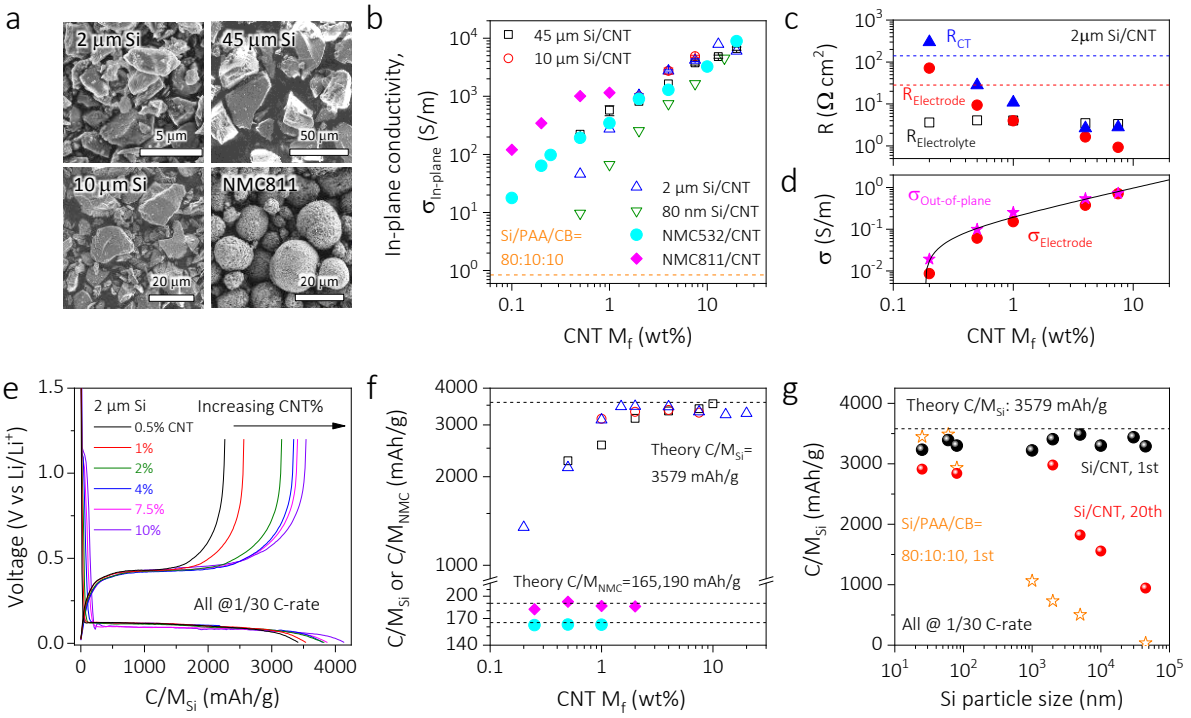

Figure 2. Segregated networks based on different active materials. (a) SEM images of selected Si (various sizes) and NMC particles used to form segregated network composites. **(b)** Plot of in-plane conductivity *versus* mass fraction (M_f) for both Si/CNT and NMC/CNT composites compared to a traditional 2µm-Si/PAA/CB composite (dashed line, composition given in panel). **(c)** Electrolyte ($R_{Electrolye}$), electrode ($R_{Electrode}$) and charge transfer (R_{CT}) resistances for 2µm-Si/CNT anodes, as extracted from electrochemical impedance spectroscopy (see SI), plotted *versus* M_f. The dashed lines represent $R_{Electrode}$ (red) and R_{CT} (blue) for a traditional electrode of 2µm-Si/PAA/CB. **(d)** Electrode conductivity ($\sigma_{Electrode}$, calculated from $R_{Electrode}$) and measured out-of-plane conductivity ($\sigma_{Out\text{-}of\text{-}plane}$), plotted *versus* M_f. Both data sets are consistent with percolation theory (solid line) with percolation threshold of $M_{f,c}$=0.18 wt%. All electrodes in c-d were ~60 µm thick. **(e)** First galvanostatic charge-discharge (GCD) curves of 2µm-Si/CNT composite anodes with various M_f, ranging from 0.5−10wt% and mass loading (M/A) ~3 mg cm^{-2}. Equivalent curves for NMC are in the SI. **(f)** Specific capacities (normalized to active mass, C/M_{Si} or C/M_{NMC}) of Si/CNT composites (first delithiation) with various Si sizes and NMC/CNT composites (first lithiation) for NMC 532 and NMC 811 as a function of M_f. The theoretical capacities are given as dashed lines. The legend in b also applies to f. **(g)** Delithiation capacities (cycle 1 and 20) for both Si/CNT composite anodes (with CNT M_f=7.5wt%, M/A≈3 mg cm^{-2}) and traditional anodes (cycle 1,

Si/PAA/CB = 80:10:10, M/A=1−2 mg cm^{-2}) plotted *versus* Si particle size. Dash line indicates theoretical Si capacity.

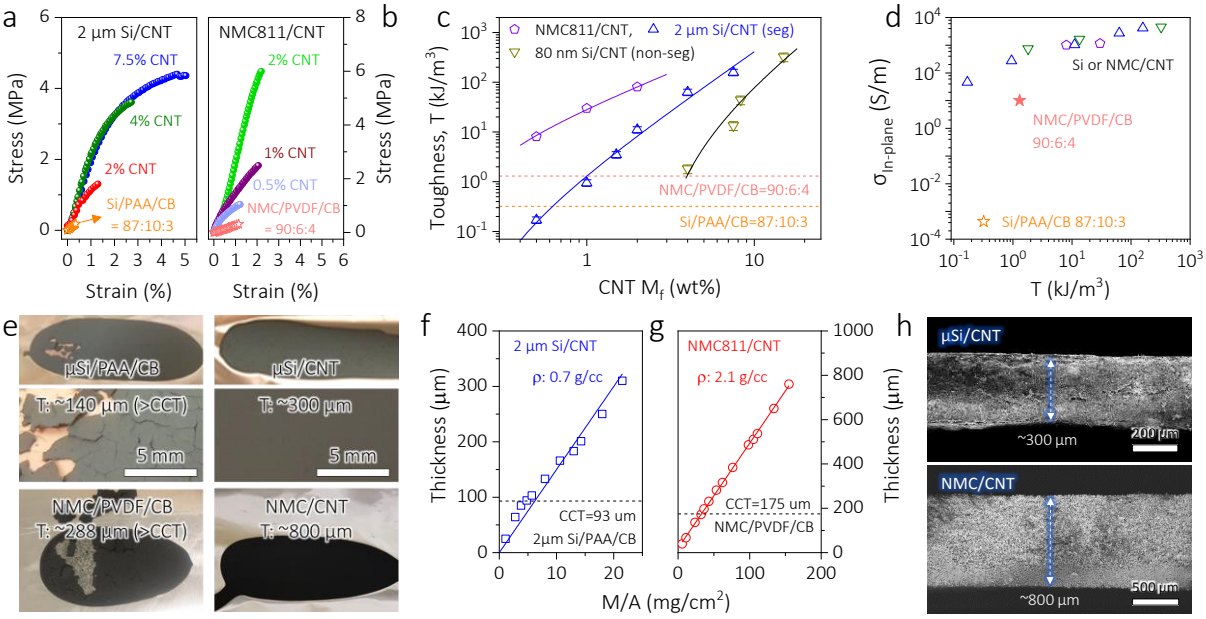

Figure 3. The effect of mechanical reinforcement on achievable thickness. (a-b) Representative stress-strain curves for 2µm Si/CNT (a) and NMC811/CNT (b) composite anodes with various CNT mass fraction (M_f). For comparison, the equivalent curves for traditional composites (active material, polymer and CB, composition given in panel) are also shown. **(c)** Tensile toughness plotted *versus* CNT M_f for segregated network composites fabricated from NMC811/CNT and 2µm Si/CNT, as well as a non-segregated network composite fabricated from 80nm Si/CNT. The solid lines are fits to percolation theory and are consistent with ($M_{f,c}$, n)= (0.15%, 1.33), (0.17%, 2.33) and (2.5%, 2.5) respectively, where $M_{f,c}$ and n is the percolation threshold and exponent. The dashed lines indicate the properties of traditional anodes (active material, polymer and CB, composition given in panel). **(d)** Plot of in-plane conductivity, $\sigma_{In\text{-}plane}$, *versus* toughness for the materials shown in **(c)**. **(e)** Photos comparing traditional electrodes prepared by polymeric binder/carbon black with segregated network electrodes. While the traditional electrodes show crack formation above their CCT, segregated network electrodes display very high CCTs allowing the formation of very thick electrodes. **(f-g)** Electrode thickness as a function of electrode mass loading, M/A, for 2µm Si/7.5% CNT and NMC811/0.25wt% CNT composites. Note that these composites can be

prepared at very high thickness. The reciprocal of slope indicates the electrode density as indicated in the panel. **(h)** Cross-sectional SEM image of the thickest composites.

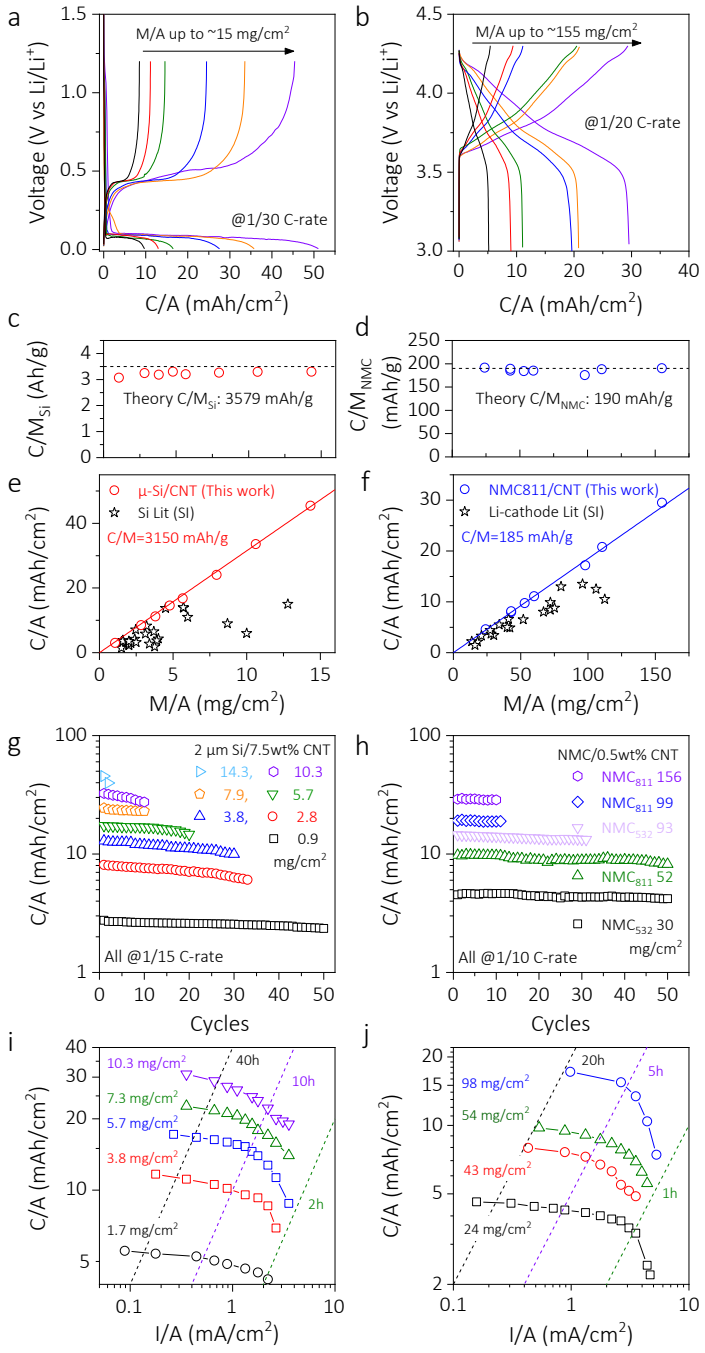

Figure 4. Electrochemical characterization of segregated network electrodes with high mass loading. (a-b) First GCD curves of (a) 2μm Si/7.5wt% CNT composite anodes for a range of areal mass density (M/A) (2.3−14.3 mg cm^{-2}) and (b) NMC811/0.5wt% CNT composite cathodes for a range of M/A (19-155 mg cm^{-2}). N.B. composite anodes with M/A>15 mg cm^{-2} couldn't be tested in half-cells, due to the insufficient Li supply from the Li-metal counter electrode. **(c-d)** Specific capacity (normalized to Si or NMC mass, C/M_{Si} or C/M_{NMC}) of the (c) 2μm Si/7.5wt% CNT anode and (d) NMC811/0.5wt% CNT cathode plotted *versus* M/A. The dash lines indicate the theoretical capacities. (**e-f**) Areal capacity, C/A versus M/A

for the data in c-d. High-performance literature data are included for comparison with the details indicated in Supplementary Table 2. **(g-h)** Half-cell cycling performance for (g) the 2μm Si/7.5wt% CNT anodes and (h) NMC811/0.5wt% CNT cathodes for a range of electrodes with different M/A, all measured at ~1/15 or ~1/10 C-rate. **(i-j)** C/A of (i) 2μm Si/7.5wt% CNT anodes and (j) NMC811/0.5wt% CNT cathodes with various M/A as a function of areal current density (I/A). The dash lines represent the actual discharge time (hour), estimated from t=(C/A)/(I/A).

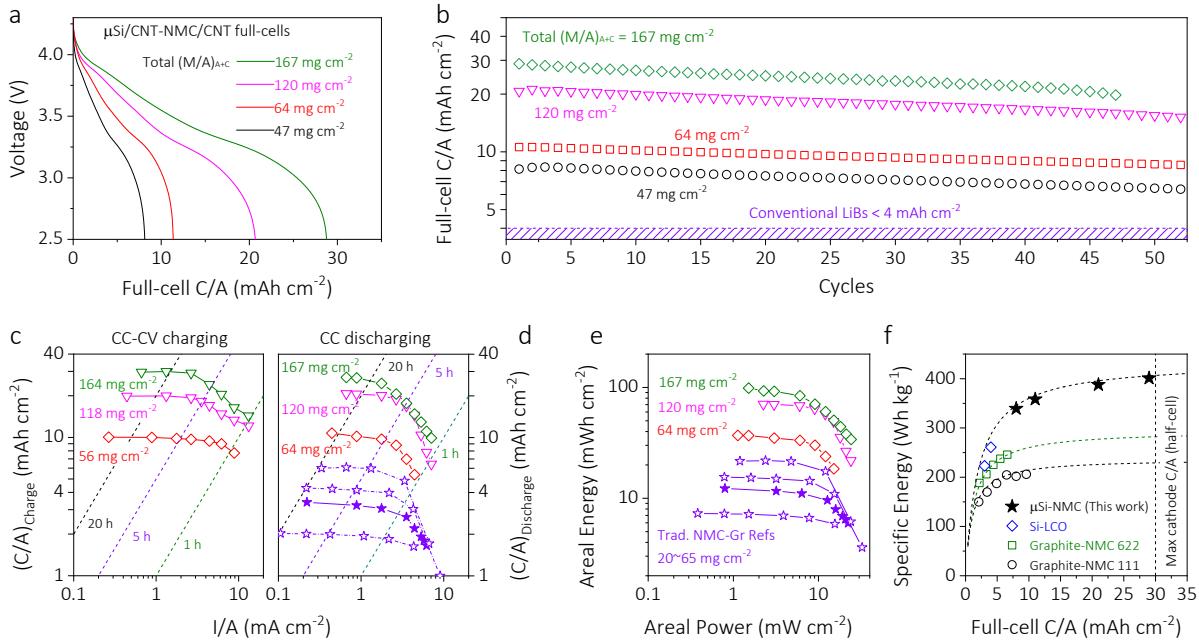

Figure 5. Electrochemical performance of full-cell lithium-ion batteries made by pairing 2μ-Si/7.5wt%CNT composite anodes with NMC811/0.5wt%CNT composite cathodes. Total anode and cathode masses, $(M/A)_{A+C}$ varied from 47 to 167 mg cm^{-2}. **(a)** Second discharge voltage–capacity curves for full-cells of varying $(M/A)_{A+C}$ tested at ~1/15 C-rate. **(b)** Cycling stability of full-cells with various $(M/A)_{A+C}$ (~1/15 C-rate). Commercial high-energy batteries typically have a maximum full-cell areal capacity (C/A) of ~4 mAh cm^{-2}, as indicated by the violet hatched area. **(c-d)** Rate performance of full-cells with various $(M/A)_{A+C}$ with a traditional NMC-graphite full-cells for comparison. Panel c represents charging measurements made in constant current-constant voltage (CC-CV) mode, while panel d represents discharging measurements made in constant current (CC) mode (see more detailed protocols in Methods). Violet stars in (d) indicate traditional NMC-Graphite full-cells made by us (closed violet star) and from literatures (open violet stars). The dash lines indicate the actual charge/discharge time estimated from t=(C/A)/(I/A). **(e)** Ragone plot calculated using the data in d. **(f)** Specific energy as a function of full-cell C/A (this work = black stars) with various literature data for comparison (open symbols, see Supplementary Table 6). The dashed lines are plots of equation 1.

References

1 Dunn, B., Kamath, H. & Tarascon, J.M. Electrical Energy Storage for the Grid: A Battery of Choices. *Science* **334**, 928-935, (2011).

2 Chiu, R.C., Garino, T.J. & Cima, M.J. Drying of Granular Ceramic Films. 1. Effect of Processing Variables on Cracking Behavior. *J. Am. Ceram. Soc.* **76**, 2257-2264, (1993).

3 Singh, K.B. & Tirumkudulu, M.S. Cracking in drying colloidal films. *Phys. Rev. Lett.* **98**, (2007).

4 Danner, T. *et al.* Thick electrodes for Li-ion batteries: A model based analysis. *J. Power Sources* **334**, 191-201, (2016).

5 Wang, G.P., Zhang, Q.T., Yu, Z.L. & Qu, M.Z. The effect of different kinds of nano-carbon conductive additives in lithium ion batteries on the resistance and electrochemical behavior of the LiCoO2 composite cathodes. *Solid State Ionics* **179**, 263-268, (2008).

6 Ruiyuan Tian *et al.* Quantifying the factors limiting rate-performance in battery electrodes. *Nature Communications (in press)* **DOI:10.1038/s41467-019-09792-9**, (2018).

7 Higgins, T.M. *et al.* A Commercial Conducting Polymer as Both Binder and Conductive Additive for Silicon Nanoparticle-Based Lithium-Ion Battery Negative Electrodes. *ACS Nano* **10**, 3702-3713, (2016).

8 Sander, J.S. *et al.* High-performance battery electrodes via magnetic templating. *Nature Energy* **1**, 16099, (2016).

9 Salvatierra, R.V. *et al.* Silicon Nanowires and Lithium Cobalt Oxide Nanowires in Graphene Nanoribbon Papers for Full Lithium Ion Battery. *Adv. Energy Mater.* **6**, 1600918-n/a, (2016).

10 Peled, E. *et al.* Tissue-like Silicon Nanowires-Based Three-Dimensional Anodes for High-Capacity Lithium Ion Batteries. *Nano Lett.* **15**, 3907-3916, (2015).

11 Leveau, L. *et al.* Silicon nano-trees as high areal capacity anodes for lithium-ion batteries. *J. Power Sources* **316**, 1-7, (2016).

12 Yang, G.F., Song, K.Y. & Joo, S.K. Ultra-thick Li-ion battery electrodes using different cell size of metal foam current collectors. *RSC Adv.* **5**, 16702-16706, (2015).

13 Wang, J.S. *et al.* Formulation and characterization of ultra-thick electrodes for high energy lithium-ion batteries employing tailored metal foams. *J. Power Sources* **196**, 8714-8718, (2011).

14 Hu, L.B. *et al.* Lithium-Ion Textile Batteries with Large Areal Mass Loading. *Adv. Energy Mater.* **1**, 1012-1017, (2011).

15 Elango, R. *et al.* Thick Binder-Free Electrodes for Li–Ion Battery Fabricated Using Templating Approach and Spark Plasma Sintering Reveals High Areal Capacity. *Adv. Energy Mater.*, n/a-n/a.

16 Choi, M.J. *et al.* Novel strategy to improve the Li-storage performance of micro silicon anodes. *J. Power Sources* **348**, 302-310, (2017).

17 Zhang, C.F. *et al.* Enabling Flexible Heterostructures for Li-Ion Battery Anodes Based on Nanotube and Liquid-Phase Exfoliated 2D Gallium Chalcogenide Nanosheet Colloidal Solutions. *Small* **13**, (2017).

18 Liu, Y.P. *et al.* Electrical, Mechanical, and Capacity Percolation Leads to High-Performance MoS2/Nanotube Composite Lithium Ion Battery Electrodes. *ACS Nano* **10**, 5980-5990, (2016).

19 Jurewicz, I. *et al.* Locking Carbon Nanotubes in Confined Lattice Geometries - A Route to Low Percolation in Conducting Composites. *J. Phys. Chem. B* **115**, 6395-6400, (2011).

20 Sundaram, R.M. & Windle, A.H. One-step purification of direct-spun CNT fibers by post-production sonication. *Mater. Des.* **126**, 85-90, (2017).

21 Gabbett, C. *et al.* The Effect of Network Formation on the Mechanical Properties of 1D:2D Nano:Nano Composites. *Chem. Mater.* **30**, 5245-5255, (2018).

22 Ge, H.C. & Wang, J.C. Ear-like poly (acrylic acid)-activated carbon nanocomposite: A highly efficient adsorbent for removal of Cd(II) from aqueous solutions. *Chemosphere* **169**, 443-449, (2017).

23 Wang, W. *et al.* Silicon Decorated Cone Shaped Carbon Nanotube Clusters for Lithium Ion Battery Anodes. *Small* **10**, 3389-3396, (2014).

24 Zhang, L. *et al.* A coordinatively cross-linked polymeric network as a functional binder for high-performance silicon submicro-particle anodes in lithium-ion batteries. *J. Mater. Chem. C.* **2**, 19036-19045, (2014).
25 Assresahegn, B.D. & Belanger, D. Effects of the Formulations of Silicon-Based Composite Anodes on their Mechanical, Storage, and Electrochemical Properties. *Chemsuschem* **10**, 4080-4089, (2017).
26 Li, X.L. *et al.* Mesoporous silicon sponge as an anti-pulverization structure for high-performance lithium-ion battery anodes. *Nature Commun.* **5**, (2014).
27 Yan, L.J. *et al.* In Situ Wrapping Si Nanoparticles with 2D Carbon Nanosheets as High-Areal-Capacity Anode for Lithium-Ion Batteries. *ACS Appl. Mater. Interfaces* **9**, 38159-38164, (2017).
28 Krause, A. *et al.* High Area Capacity Lithium-Sulfur Full-cell Battery with Prelitiathed Silicon Nanowire-Carbon Anodes for Long Cycling Stability. *Sci. Rep.* **6**, (2016).
29 Li, B., Li, S.M., Xu, J.J. & Yang, S.B. A new configured lithiated silicon-sulfur battery built on 3D graphene with superior electrochemical performances. *Energy Environ. Sci.* **9**, 2025-2030, (2016).
30 Shi, F.F. *et al.* Failure mechanisms of single-crystal silicon electrodes in lithium-ion batteries. *Nature Commun.* **7**, (2016).
31 Nguyen, C.C. & Lucht, B.L. Development of Electrolytes for Si-Graphite Composite Electrodes. *J. Electrochem. Soc.* **165**, A2154-A2161, (2018).
32 Singh, M., Kaiser, J. & Hahn, H. Thick Electrodes for High Energy Lithium Ion Batteries. *J. Electrochem. Soc.* **162**, A1196-A1201, (2015).
33 Singh, M., Kaiser, J. & Hahn, H. A systematic study of thick electrodes for high energy lithium ion batteries. *J. Electroanal. Chem.* **782**, 245-249, (2016).
34 Gallagher, K.G. *et al.* Optimizing Areal Capacities through Understanding the Limitations of Lithium-Ion Electrodes. *J. Electrochem. Soc.* **163**, A138-A149, (2016).
35 Purvins, A., Papaioannou, I.T. & Debarberis, L. Application of battery-based storage systems in household-demand smoothening in electricity-distribution grids. *Energy Conversion and Management* **65**, 272-284, (2013).
36 Yamada, M. *et al.* Performance of the "SiO"-carbon composite-negative electrodes for high-capacity lithium-ion batteries; prototype 14500 batteries. *J. Power Sources* **225**, 221-225, (2013).
37 Son, I.H. *et al.* Silicon carbide-free graphene growth on silicon for lithium-ion battery with high volumetric energy density. *Nature Commun.* **6**, (2015).
38 Ma, L. *et al.* A Guide to Ethylene Carbonate-Free Electrolyte Making for Li-Ion Cells. *J. Electrochem. Soc.* **164**, A5008-A5018, (2017).